Available online at www.sciencedirect.com
ScienceDirect
Journal of Sound and Vibration 313 (2008) 375–394
JOURNAL OF SOUND AND VIBRATION
www.elsevier.com/locate/jsvi

An event-based vibration control for a two-link flexible robotic arm: Numerical and experimental observations

Abdullah Özer, S. Eren Semercigil*

School of Architectural, Civil and Mechanical Engineering, Victoria University, Footscray Park Campus, P.O. Box 14428, MCMC, Melbourne, Vic. 8001, Australia

Received 13 February 2006; received in revised form 16 August 2006; accepted 16 September 2006
Available online 14 March 2008

Abstract

Flexible robot manipulators have numerous advantages over their rigid counterparts. They have increased payload-to-weight ratio, they run at higher speeds, use less energy and smaller actuators, and they are safer during interaction with their environments. On the other hand, light design combined with external effects result in components which can oscillate with excessive amplitudes. These oscillations cause deviation from the desired path and long idle periods between tasks in order to perform the intended operation safely and accurately. This paper is on an investigation into the effectiveness of a vibration control technique for a two-link flexible robotic arm. Variable stiffness control (VSC) technique is used to control the excessive oscillations. Owing to its dissipative nature, the technique is stable, it is relatively insensitive to significant parameter changes and suitable to be implemented on existing robots. This research considers that the source of the flexibility is either the joints or the links or both. Simulation results of the response of the arm are presented to show the versatility of the proposed control technique. Experiments are performed on a laboratory prototype and the results are presented to test the validity of simulations.

1. Introduction

With the increasing demand and importance of robots in industry and space applications, many researchers have focused on the modeling and control aspects of robot manipulators in recent years. First generation robots in industry were built as massive, rigid structures for accuracy. These first generation robots ran at low speeds, consuming wasteful energy resulting in inefficiency in industry. New generation robots need to be lighter, therefore more flexible, for improved productivity and increased payload-to-weight ratio. However, the increased payload-to-weight ratio of these new generation robots will cause undesirable deflections during an operation, which make the controllability of the robotic arm more challenging. The source of flexibility in these new generation robots can be either at joints (coming from the electromechanical drives, in series with other units such as harmonic drives, couplings and belt drives) or from their slender linkages.

*Corresponding author.
E-mail address: eren.semercigil@vu.edu.au (S. Eren Semercigil).

0022-460X/$ - see front matter © 2006 Published by Elsevier Ltd.
doi:10.1016/j.jsv.2006.09.021

Light design combined with high speeds or interacting with surrounding objects or by stopping abruptly once a new positioning completed may be a source of disturbance to cause these oscillations. If not controlled effectively, these oscillations not only lead to end point positioning and tracking inaccuracies but also cause long idle waiting periods between tasks to perform the intended operation safely and accurately. Hence, controlling the vibrations of robots with flexibility is a problem of practical significance.

Vibration control of flexible manipulators has received considerable attention in the literature. The control techniques developed in the literature can be grouped into two main categories: passive control techniques and active control techniques. Generally, passive control techniques have limited effectiveness for this particular problem. A passive controller aims at designing the mass, stiffness and energy dissipation properties of structures to minimize dynamic response. Their primary advantage is simplicity. However, the effectiveness of a passive vibration controller may deteriorate drastically for varying design conditions [1–4]. In addition, passive controllers generally tend to be bulky.

Active vibration control techniques adopt an entirely different approach than that of passive techniques. An active controller senses the response, generates and imposes the required corrective forces using actuators. Hence, stability of the control technique cannot always be guaranteed, since energy is added for control purposes. Also, performance of most of the active vibration control techniques for robots with flexible members, rely on a proper dynamic model. This need may cause difficulties since there are unavoidable simplifications in models. In addition, dynamics of a robot could change significantly by an operation such as picking up a payload or changing relative orientation of linkages. Therefore, it is very important to use a vibration control technique whose performance is relatively independent from the system parameters. Thus, modeling and measurement inaccuracies may lead to unstable control resulting in exaggeration rather than attenuation of the oscillation amplitudes. However, active controllers are significantly more versatile and smaller than passive controllers.

Active vibration control of robotic structures has been an active research area over the past 10 years or so. Bernzen [5] used an active control technique based on employing the actuators as virtual spring–damper systems. As the spring–damper element is passive, the control action cannot destabilize the system, and it should be insensitive to modeling errors. To achieve the control, the value of the optimal damping was adjusted to maximize the energy dissipation for each stiffness constant. However, controller's performance becomes an issue for more complex structures, where a model is unavailable or difficult. Siciliano [6] used inverse kinematics approach to find the joint and deflection variables for a given tip position, and a constraining force from a contact surface. The Jacobian employed in the algorithm was obtained by correcting the equivalent rigid manipulator Jacobian, with two terms that account for the static deflections due to gravity and contact force. The procedure has been tested on a two-link arm. The scheme was restricted for a flexible manipulator under gravity whose tip is constrained by a stiff surface. Yuan [7] has investigated an active and robust vibration control technique based on identified models. The technique was suitable for applications where modal parameters, such as eigenfunctions or mass/stiffness coefficients are not available analytically. However, stability may not be guaranteed with this technique, and it is highly demanding in terms of measurement and complex computational requirements during identification and control.

Adaptive control techniques can be helpful by tuning the controller gains where system parameters change significantly during the operation. Lim et al. [8] presented an adaptive partial state-feedback controller for a rigid-link flexible-joint arm. The controller compensates for parametric uncertainty while only requiring measurement of link position and actuator position. Bartolini et al. [9] formulated a model of a simple robotic structure and applied the sliding modes concept when velocities, positions and the elastic forces are known. In cases where the time delay in the actuation forces does not allow an ideal sliding mode control, they used discontinuous control law with adaptive gain. Both the large computational requirements and the large number of feedback parameters can make these adaptive control techniques impractical.

Apart from attempting the control of excessive oscillations of flexible robots, some of the work in the literature only deal with the theory of modeling and control. The reason for this purely theoretical treatment of the problem was either to support the research in the area, or because there were some practical problems in application (such as difficulties in sensing the feedback and large volume of computations required to decide the corrective action). Maxwell and Asokanthan [10] have studied the modal characteristics of a flexible beam with multiple distributed actuators. They developed a generic model for a vibrating cantilever beam with

surface-bonded piezo-ceramic patches using Timoshenko beam theory and Hamilton's principle. The effect of patch placement has been discussed on the modal characteristics with numerical examples. However, no control strategy has been attempted on vibration control of a flexible beam. Mohamed and Tokhi [11] have investigated feed-forward control strategies for vibration control of flexible manipulators using command shaping techniques based on input shaping, low pass and band-stop filtering. In this study, single-link flexible robot manipulator has been considered and the dynamic model of the system has been derived using finite-element method. The input shapers and filters were designed based on the properties of the manipulator and used for pre-processing the input, so that no energy is put into the system at resonance modes. While significant reduction in the system vibrations has been achieved numerically, computational complexity (consequently the execution times to develop the shaped and filtered inputs) was the main concern.

The problem with flexible robot manipulators is that they are difficult to control and susceptible to vibrations induced by movement of the robot itself or by external disturbances. On the other hand, the many degrees of freedom involved, make the control of coupled system a complex task. A compromise between the active and passive vibration controllers is the semi-active control. Semi-active controllers offer significant simplification over active controllers. A semi-active system operates on the premise that varying conditions require different passive controllers to be effective. Hence, an effective control may be achieved by varying the parameters of the otherwise passive system, rather than imposing control with force actuators. Therefore, control effort is quite minimal. The work presented in this paper utilizes a semi-active technique.

Semi-active controllers have been used widely to control the oscillations of engineering structures. Lu [12] studied a semi-active modal control strategy for seismic structures with variable friction dampers. The method aimed to reduce the floor displacements and accelerations by installing semi-active friction dampers to a structure. Owing to the energy dissipation property of the proposed technique, significant improvement has been observed as compared to passive friction dampers. Kim and Lee [13] used a semi-active damping control for a suspension system of a cabin. The control strategy has aimed to maximize the energy dissipation rate. They designed a control strategy that minimizes the cabin oscillations for an operational response mode without necessitating accurate system parameters and dynamics. They reported the reduction of the responses by the proposed on–off control system with comparisons of the original system, passive control system and sky-hook control system via a numerical example. Zhou et al. [14] investigated magnetorheological (MR) dampers to control the vibrations of three-dimensional (3-D) inclined sag cable. A semi-active control strategy based on the modulated homogeneous friction algorithm has been used. The vibration reduction capability of the proposed MR dampers is demonstrated by comparison with an optimal viscous damper. Liu et al. [15] presented a comparison study on semi- active control strategies for vibration isolation purposes. Several control algorithms based on skyhook control, balance control, and adaptive damping control are numerically tested. Their study concluded that the semi-active systems could always provide better isolation at higher frequencies than a conventional passive damped system.

Prior research has already indicated the potential of the variable stiffness control (VSC) technique. Onoda et al. [16] have demonstrated that oscillations of a cantilever truss-beam can be controlled by varying the stiffness of selected members using piezo-electric actuators. Warkentin and Semercigil [17] and Pun and Semercigil [18] demonstrated the effectiveness of VSC technique on robotic arms by employing auxiliary passive components to implement the control action. One of the major limitation of the two attempts in Refs. [17,18], is their requirement of additional hardware. The objective here is to implement the control without necessitating any additional hardware and complex computational requirements. This will provide a good base of extension of the proposed controller's applications (such as employing the control for a maneuvering arm or during machining processes to delay dynamic instabilities associated to waste removal).

The proposed technique is based on manipulating the joint resilience, which is inherent (to a certain degree) in the structure. The actuation is timed with a ''kinematic event'', namely the instant of peak displacement, rather than the structural dynamics. This point will be further clarified in the next section. Hence, the control performance is independent of system parameters. It is stable. It is suitable to be implemented as an add-on controller to arms with many degrees of freedom.

It should be mentioned here that no claims are made for superior effectiveness. There may well be more effective, and arguably more complex, existing active control techniques. However, the suggested method is

simple, stable and will require no additional hardware to provide effective control. In the next sections, the proposed control technique will be presented with observations from simulations and experiments.

2. Numerical model and control method

2.1. VSC technique

In this section, the VSC technique, will be described using a single degree of freedom mechanical oscillator as shown in Fig. 1. The technique can be summarized as one that combines the unconditional stability of a passive system with the performance of an active control technique with much smaller computational and hardware requirements. The VSC technique is based on changing the stiffness of the system between two states at instances when it is most beneficial for control.

The undamped oscillator shown in Fig. 1, has two parallel springs, a passive spring with a stiffness of K–ΔK and an active spring with ΔK. Effective stiffness of the system is K when the clamp of the active spring is applied, and K–ΔK when the clamp is released. M represents the mass of the oscillator, coordinate x indicates the absolute displacement.

For the system shown in Fig. 1, the equation of motion for free vibration is

$$M\ddot{x} + Kx = \Delta K x^*, \tag{1}$$

where $\ddot{x}$ represents the second time derivative of x. Here x^* represents the displacement of the system at the instant of control action where the clamp is actuated. Initially, the active spring is clamped producing the full stiffness K. After applying a transient disturbance to start oscillations of the system, the active spring is kept clamped until the instant of peak displacement X_0. For maximum energy dissipation, at the instant of peak displacement the active spring is unclamped. By this unclamping action, the active spring instantaneously releases all the potential energy gained until reaching to this peak point. At this instant, while the oscillator is still at its peak position, the active spring is re-clamped.

Along with this dissipated energy, the active spring is now in an undeformed state when the clamp is re-applied instantaneously while the oscillator is still displaced by X_0. The shifted equilibrium position imposes a constant restoring force of amplitude "$\Delta K^* X_0$" to oppose the velocity of oscillations. Similar to the case of Coulomb friction, the solution of Eq. (1) can be obtained as

$$x(t) = A_n \cos(\omega_n t) + B_n \sin(\omega_n t) + \frac{\Delta K}{K} x^*, \tag{2}$$

where ω_n, A_n and B_n are the undamped natural frequency and the arbitrary integration constants. With the assumption of zero initial displacement and an initial velocity of ωX_0, the solution simplifies to

$$x(t) = X_0 \sin(\omega_n t). \tag{3}$$

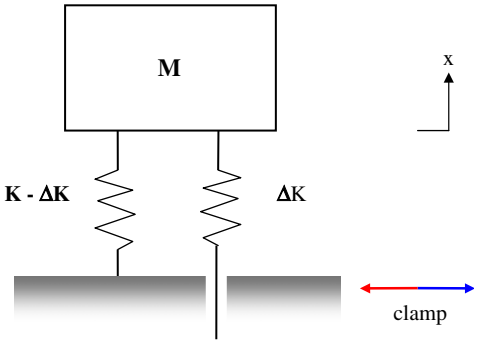

Fig. 1. Undamped oscillator with variable stiffness control.

After repeated evaluation of integration constants, the response can be generalized after n successive actuation as

$$x(t-t^{*n}) = X_0\left(\frac{2\Delta K}{K}-1\right)^{n-1}\left[\left(1-\frac{\Delta K}{K}\right)\cos(\omega_n(t-t^{*n}))+\frac{\Delta K}{K}\right]. \quad (4)$$

The most effective stiffness ratio, $\Delta K/K$, is 0.5 which would eliminate the transient oscillations of an undamped oscillator in just two actuations [16–18].

The effect of the control action may also be shown clearly in the force-displacement diagram in Fig. 2. Oscillations start at the origin when the external disturbance is imposed and follow State 1 with full stiffness K until the maximum displacement X_0. At X_0, the active spring is unclamped and the system jumps from "a" to "b", into State 2 with an effective stiffness of K–ΔK. When the active spring recovers, the effective stiffness again becomes K and oscillations resume in State 3. Potential energy dissipated by the control action is represented by the area of the trapezoid bounded by States a, b and the two parallel lines representing the full stiffness K (States 1 and 3) in the first quadrant. The equilibrium shift that produces the constant restoring force is the result of shift in the state of the system from State 1 to State 3. The shifted equilibrium position will be at a smaller displacement amplitude for the second and following actuations of the control, eventually leading to a zero displacement off-set when oscillations diminish.

It is important to note that the VSC technique is always dissipative. An actuation never results in an addition of energy to the system. Therefore, the control technique is unconditionally stable for a lumped parameter oscillator.

Fig. 3 shows the model of the arm investigated in this paper. The arm consists of two flexible beams. Link-2 is attached to Link-1 at elbow, and Link-1 is attached to base with pin joints. Two parallel torsional springs, at elbow and base, represent active and passive springs similar to the single degree-of-freedom model discussed earlier. Control is achieved by switching these active springs off-and-on at the peak angular displacement instances.

The passive springs, K_{elbow}–ΔK_{elbow} and K_{base}–ΔK_{base}, represent compliant elbow and base joints while the second torsional springs, ΔK_{elbow} and ΔK_{base}, model the active springs of the controller. Torsional viscous dampers provide a model for frictional dissipation at joints which are not shown in the figure for clarity. Structural damping of 0.5% of the critical damping for the first two modes is also included in the model to represent inherent energy dissipation [19]. The arm is assumed to move in the horizontal plane. Lumped masses located at the tip, M_{tip}, and at the elbow, M_{motor}, model the payload and motor mass. The rotary inertia effects at both base and elbow are neglected in the model. The mass of the base actuator is assumed to be a part of the fixed base.

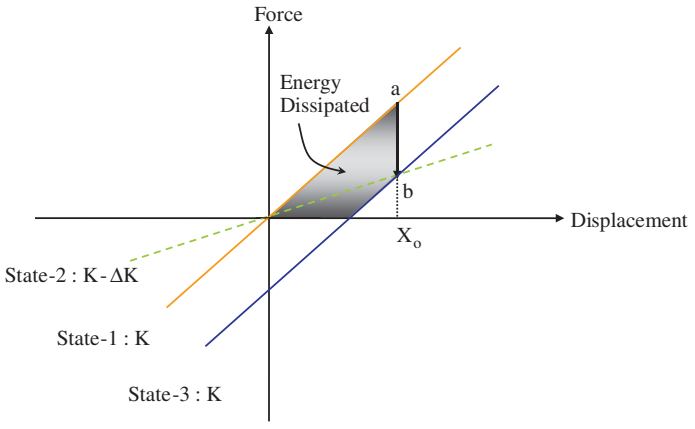

Fig. 2. Force-displacement graph of the system in Fig. 1.

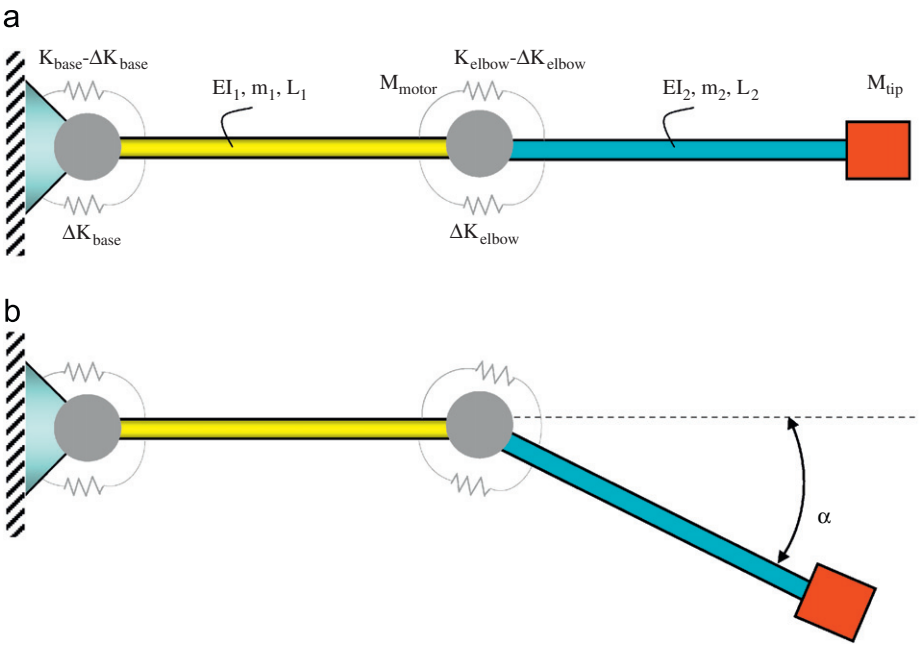

Fig. 3. Model of a two-link flexible robot arm when the linkages are: (a) aligned and (b) bent by α.

2.2. Numerical simulations

Several further simplifying assumptions have been made in the numerical model. First, only small oscillations are assumed. Secondly, to avoid the time varying system matrices, elbow angle, α, is set to a specific value before the system is excited so that the oscillations are always around prescribed position of the arm. Thirdly, the flexible arms are assumed to be Euler–Bernoulli beams. Finally, initial conditions are assumed to be zero.

Using standard finite-element method with the given parameters, a numerical model in global coordinates can be obtained for the system in matrix form as [20]

$$[M]\{\ddot{U}\} + [C]\{\dot{U}\} + [K]\{U\} = \{P(t)\}. \tag{5}$$

In Eq. (5), $[M]$, $[C]$ and $[K]$ represent global mass, damping and stiffness matrices, respectively. $\{U\}$ represents the generalized coordinate vector. $\{P(t)\}$ represents the generalized force vector. Numerical simulations are obtained using a custom coded program in MATLAB [21]. The number of finite elements for the model has been selected to be 10 for each link. Assuming the longitudinal, transverse and rotational vibrations for each beam element the system matrices have been created. Also, joint oscillations (only rotational) at the base and elbow and, lump mass parameters at the tip and elbow are superimposed to the system matrices. With this selection, the differential equation system corresponds to a vibratory system with 62 degrees of freedom. First, the program produces the global matrices. Then numerical integration is performed using the Newmark-β scheme [22].

Actuation instances are determined by monitoring relative angular velocity at joints. An actuation is performed in the time step immediately following a sign change in the relative angular velocity. The effect of an actuation in the numerical process, is to apply a constant resisting torque at the joint, after a peak relative angular displacement. This constant torque is kept until the next sign change occurs in relative angular velocity. The magnitude of the torque in each actuation, is determined from the product of the relative angular displacement at that instant and the active stiffness coefficient, ΔK. A simple low pass filter is implemented to avoid premature actuations that may be caused by higher frequencies.

As the arm folds in from 0° (straight arm) to 150°, the fundamental frequency of the system increases requiring smaller integration step as compared to that for the fully open arm. Therefore, for higher elbow

angles, a smaller integration step is needed for accuracy of numerical integration. The integration step of 0.00125 s has been found to be small enough for numerical accuracy. Integration time step has been selected to be 0.005 s for small elbow angles of up to 60°.

Simulations start with a tip disturbance of $5\sin(\omega_1 t)$ that represents an impact of the arm with its environment. This impact is a half-sinusoid, which is always perpendicular to the tip of the link-2. ω_1 is the fundamental frequency of the arm. Since the very first peak of relative elbow and/or base angle has the largest absolute value, the very first actuation will have the highest corrective torque applied in the numerical simulations. Therefore, the first actuation has a high significance over the effectiveness of the control. Due to its significant importance, a delay is implemented in the numerical process to avoid a premature first actuation. Any sign change in angular velocity is ignored until a quarter of fundamental period is reached. All the simulations run for 2 s, which is, in most cases, sufficient to observe a settling time. As a measure of the performance of the proposed controller, settling time is assumed when the tip displacement amplitudes decay below 0.001 m.

2.3. Numerical predictions

Simulations are performed for uncontrolled, elbow-only controlled, base-only controlled and dual-controlled cases to enable comparisons. In addition, results are also generated with varying elbow angles and link lengths. In order to determine the optimal stiffness ratios, number of computer simulations are also performed. The results are grouped into two subsections for flexible joint-rigid link arms and for flexible joint-flexible link arms. The same numerical procedure is used in both sub-sections. Table 1 shows the arm parameters and other parameters used for numerical simulations. All tip displacements are presented in local coordinates, perpendicular to the tip of link-2.

2.3.1. Rigid link, flexible joint arm

Most robots are powered by electro-mechanical drives, consisting of DC or AC motors in series with other units such as harmonic drives, couplings and belt drives. Flexibility, which is always inherent in these units, produces undesirable oscillations even when the linkages are selected to be as rigid structures. In this section, the effectiveness of the proposed controller on a robotic arm with flexible joints and rigid-linkages is presented.

The numerical simulations have been performed for the model shown in Fig. 3 and for the parameters given in Table 1, with the exception of increasing the bending stiffness of the arms by a factor of 10^6. The results in Figs. 4 and 5 are obtained with 0.5 stiffness ratio for both base ($\Delta K_{base}/K_{base}$) and elbow ($\Delta K_{elbow}/K_{elbow}$).

Table 1
Two link-arm parameters used for simulation

Arm parameters (same for both links)	
Length, L	0.5 m
Width of beam, b	0.05 m
Thickness of beam, h	0.00625 m
Bending stiffness of beam, EI	7.3 N m^2
Mass/length of beam, m	0.85 kg/m
Number of finite elements for each link	10
Other parameters	
Tip mass, M_{tip}	0.5 kg
Actuator mass, M_{motor}	0.5 kg
Passive elbow stiffness, K_{elbow}-ΔK_{elbow}	100 N m/rad
Active elbow stiffness, ΔK_{elbow}	100 N m/rad
Passive base stiffness, K_{base}-ΔK_{base}	200 N m/rad
Active base stiffness, ΔK_{base}	200 N m/rad
Equivalent viscous damping ratio—structural	0.005
Elbow viscous damping coefficient	0.5 N m/rad/s
Base viscous damping coefficient	0.5 N m/rad/s

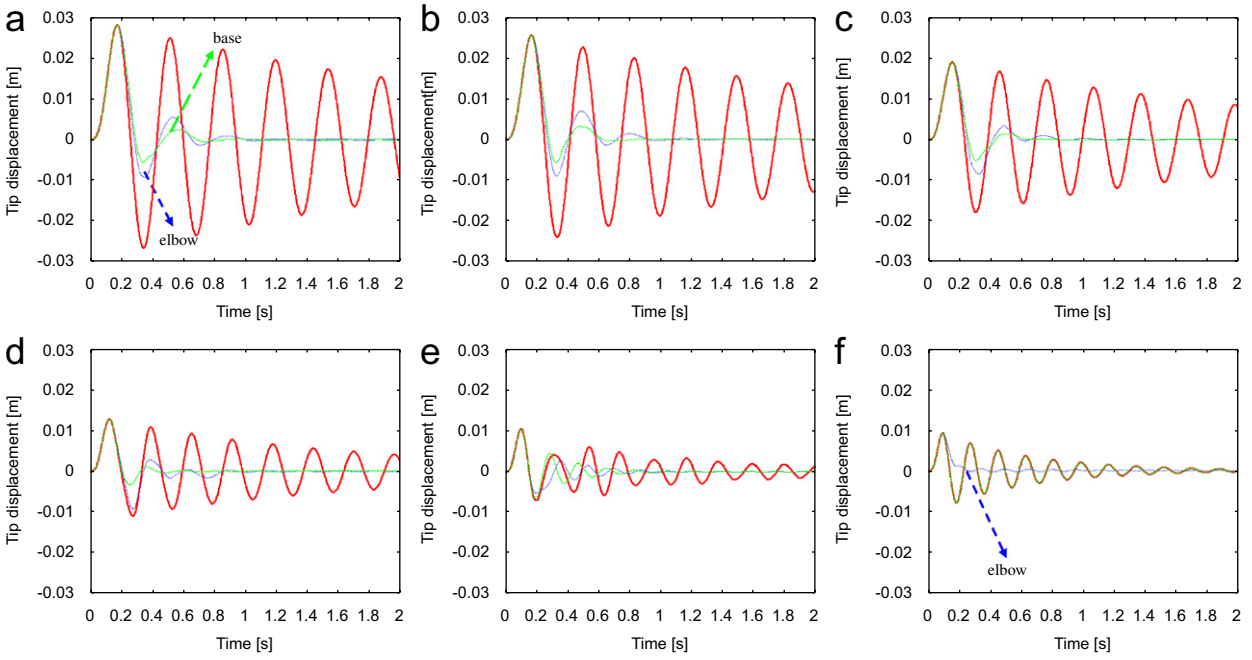

Fig. 4. Tip displacement histories of uncontrolled (—), only-elbow controlled (··· ···) and only-base controlled (- - - - -) cases for different elbow angles of: (a) $\alpha = 0^\circ$, (b) $\alpha = 30^\circ$, (c) $\alpha = 60^\circ$, (d) $\alpha = 90^\circ$, (e) $\alpha = 120^\circ$ and (f) $\alpha = 150^\circ$.

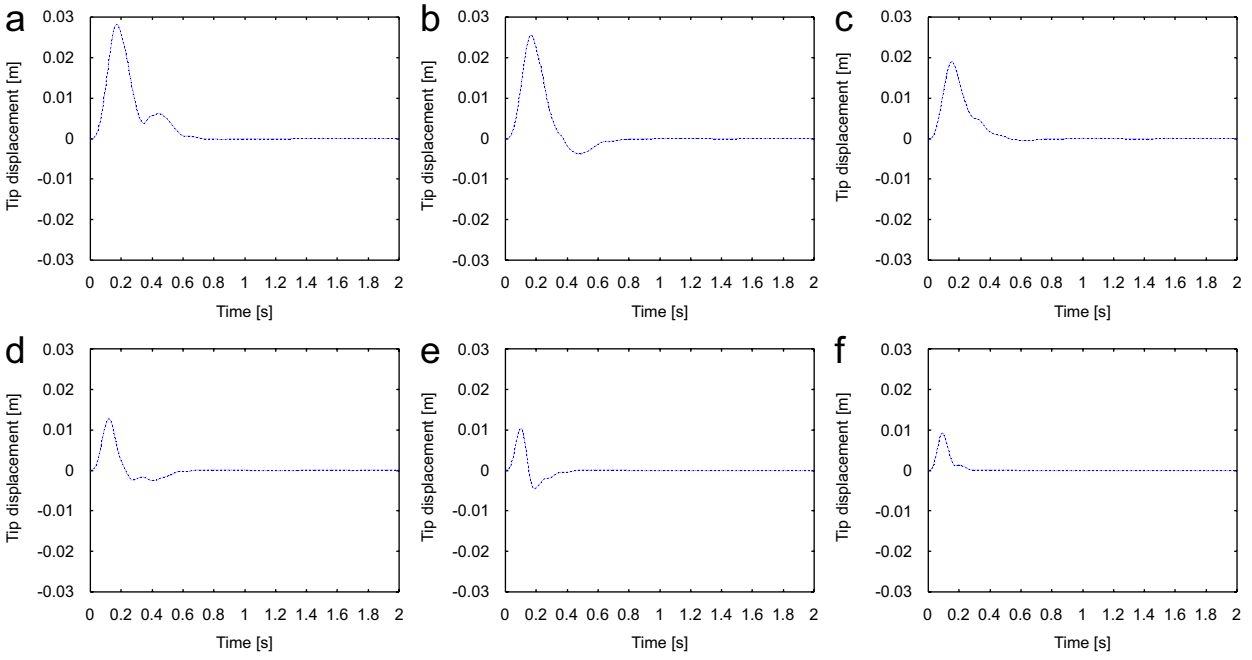

Fig. 5. Same as in Fig. 4, but for dual control.

The validity of this assumption was checked and details are presented in Ref. [23]. Histories of the tip displacement for uncontrolled (——), only-elbow (. . . . . .) and only-base controlled (- - - - - -) cases are shown in Figs. 4(a)–(f) for elbow angles, α, of 0°, 30°, 60°, 90°, 120° and 150°. In Figs. 4(a)–(f), horizontal axis represents the time and vertical axis represents the tip displacement.

Table 2
Natural frequencies of the system for different elbow angles (with rigid linkages)

Elbow angle (deg)	ω_1 (rad/s)	ω_2 (rad/s)
0	18.44	86.97
30	19.00	75.47
60	20.66	58.28
90	24.11	49.91
120	29.80	40.55
150	35.26	40.64
180	35.04	45.74

As the arm folds in, the maximum displacement amplitude decreases from around 0.03 m for 0° to around 0.01 m for 150°. In addition, the fundamental frequency of the structure increases, as presented in Table 2, from 18.44 to 35.26 rad/s for the same angles. The reason for this behavior, of course, is the increase in the apparent stiffness of the arm when it changes from a straight open arm configuration to a folded one.

In a wide range of elbow angles, from 0° to 90°, base controller cases show better effectiveness over those of the elbow controller cases. But, as the arm folds in further, the effectiveness of the elbow control over the base control becomes clearer. Especially for the 150° elbow angle, base control becomes virtually ineffective by giving almost the same performance as that of the uncontrolled case. This is not surprising, considering the fact that as the arm folds in, most of the energy is stored between the elbow and the tip of the arm after the tip impact occurs. As a result, the deflections between the elbow and the tip will be higher than those at the base. Higher deflection amplitude means higher corrective torque from the control which result in a more effective control.

In an identical format to that in Fig. 4, observations from the simulations with a dual controller (– · – · – · –) are presented in Fig. 5. Improvement over single controller is clear in almost all cases, especially at higher elbow angles around 150°. The settling time is less than 0.6 s for almost all the elbow angles. As mentioned before, settling time is assumed when the tip displacements decay below 0.001 m. With this definition, uncontrolled settling time is about 13 s at 0° elbow angle due to the poor inherent energy dissipation. Hence, dual control action at this angle shows about 22 times (95%) faster attenuation than the uncontrolled case. The percentage improvement for larger elbow angles is also comparable with that of the straight arm case (about 89% at 150°).

2.3.2. *Flexible link, flexible joint arm*

In the previous section, the effectiveness of the proposed control technique has been demonstrated for the flexible-joint and rigid-link arm model. Such a system may be characterized as a lumped parameter system, as the model does not include flexural vibrations of the beams. In order to show the effectiveness of the VSC technique over flexural vibrations along with the vibrations at joints, simulations are presented in this section with flexible beams.

Fig. 3 again represents the investigated model. Results in this section have been obtained using the same parameters in Table 1, each link consisting of a thin 0.5 m long aluminum beam. Damping coefficients are increased to 1 N m/rad/s for the elbow, and 3 N m/rad/s for the base owing to the potential buckling effects of the arms at each motor axis.

Histories of the tip displacement for uncontrolled (——), only-elbow (⋯ ⋯) and only-base controlled (- - - - - -) cases are given in Fig. 6 in an identical format to that of Fig. 4. The stiffness ratio, $\Delta K_{\text{base}}/K_{\text{base}}$ or $\Delta K_{\text{elbow}}/K_{\text{elbow}}$, for controlled cases has been selected to be 0.5. Justification of this choice is again detailed in Ref. [23].

As the arm folds in, the maximum displacement amplitudes decrease from around 0.06 m for 0° to around 0.02 m for 150°. In addition, the fundamental frequency of oscillations increases, as presented in Table 3, from 12.52 to 24.59 rad/s for the same angles. While fundamental frequency of the system increases, as the arm folds in from 0° to 150°, second frequency decreases from 66.95 to 31.49 rad/s, placing the first and second

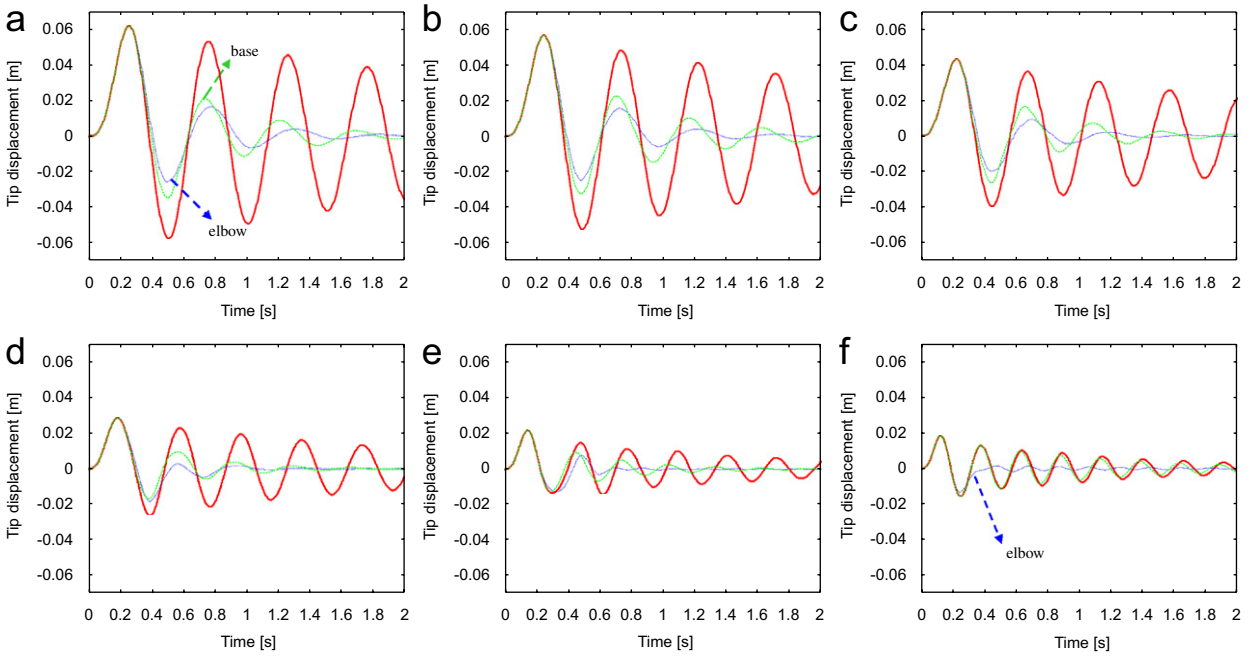

Fig. 6. Tip displacement histories of uncontrolled (——), only-elbow controlled (⋯ ⋯) and only-base controlled (- - - - - -) cases for different elbow angles of: (a) $\alpha = 0^\circ$, (b) $\alpha = 30^\circ$, (c) $\alpha = 60^\circ$, (d) $\alpha = 90^\circ$, (e) $\alpha = 120^\circ$ and (f) $\alpha = 150^\circ$.

Table 3
Natural frequencies of the system for different elbow angles (with flexible linkages)

Elbow angle (deg)	ω_1 (rad/s)	ω_2 (rad/s)
0	12.52	66.95
30	12.88	58.61
60	14.05	45.81
90	16.30	37.13
120	20.08	32.38
150	24.59	31.49
180	25.84	33.66

frequencies closer at higher elbow angles. At 180°, there is a slight increase in the second frequency for the fully folded arm.

In Figs. 6(a)–(c), between 0° and 60° elbow angles, the effectiveness of both controls are comparable. But, as the arm folds in further, the effectiveness of the elbow control over the base control becomes clearer. Especially in Fig. 6(f), at an angle of 150°, only-base control becomes ineffective by giving almost the same performance as that of the uncontrolled case. Similar observation was also made with rigid-link, flexible-joint case in the preceding section, and a parallel interpretation of such behavior is also valid here. In an identical format to that in Fig. 6, results of the simulations with a dual controller (–·–·–·–) are presented in Fig. 7.

Improvement with dual-control is clear in almost all cases, especially at large elbow angles. The settling time is less than 1 s and at almost all the elbow angles, whereas the uncontrolled settling time is about 15 s at 0° elbow angle. Hence, dual control action at this angle shows about 15 times (93%) faster attenuation than the uncontrolled case. This is about twice as fast as those of both of the single control actions. Similar performance is also valid for higher elbow angles, with 89% faster attenuation at 150°.

In addition to above simulations, to demonstrate the relative insensitivity of the control method to significant parameter changes, the arm lengths have been varied while keeping all the other parameters the

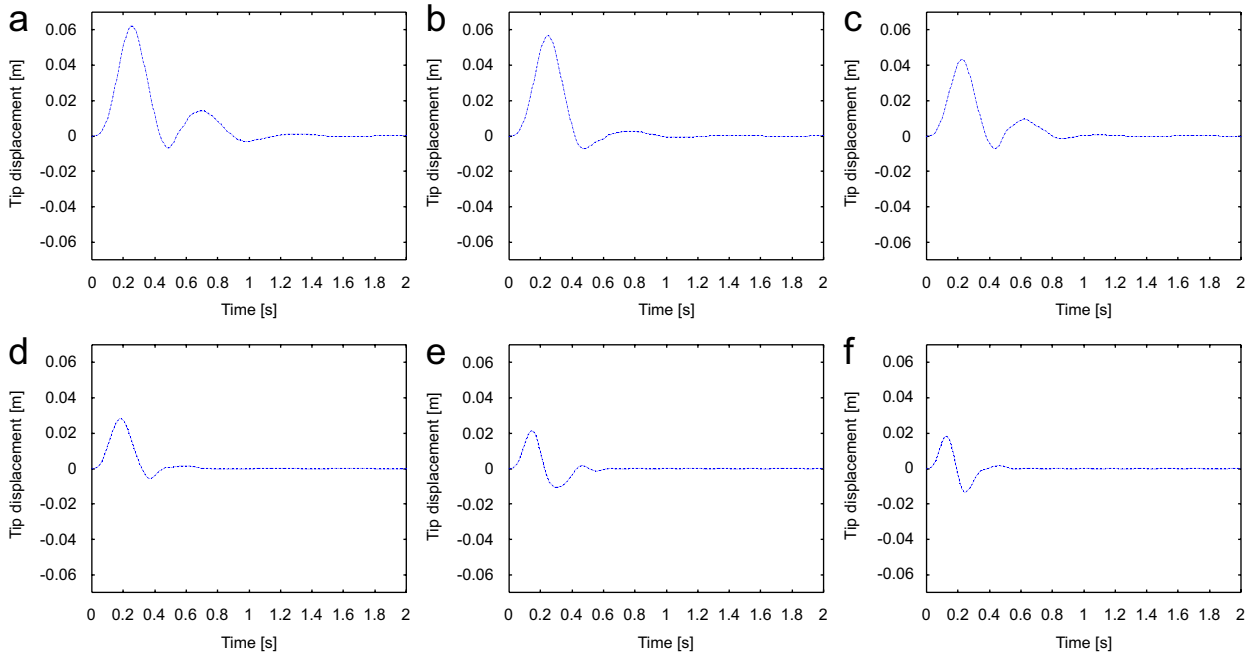

Fig. 7. Same as in Fig. 6, but for dual control.

same as before. In Fig. 8, results are presented for the 0° elbow angle for the dual control case (–·–·–·–) and the uncontrolled case (——). In Figs. 8(a) and (c), the length of link-1 (L_1) has been changed from 0.5 to 0.2 m while keeping all other parameters the same for rigid and flexible linkages, respectively. Similarly, in Figs. 8(b) and (d), results are shown this time by changing only the length of link-2 (L_2) from 0.5 to 0.2 m for rigid and flexible linkages. The method is relatively insensitive to structural parameters with significant attenuations as compared to the uncontrolled cases. This length change could be representative for telescopic robot arms.

3. Experiments

The primary objective of this section is to validate the numerical predictions and show the applicability of the proposed controller to existing robots. The results of experimental findings are presented in a similar way to verify the simulation results. First the experimental setup and procedure will be described. Then, the implementation of the VSC technique will be discussed. The experimental results for a two-link robot arm will be presented for only-elbow, only-base and dual-control cases with different elbow angles.

3.1. Experimental setup and procedure

A schematic overview and a photograph of the laboratory setup are shown in Figs. 9(a) and (b), respectively. The laboratory setup consists of a two-link arm (items a and b), payload mass at the tip of the arm (item c), and connection elements for supporting the load and the actuators, a personal computer (d) (Pentium II with PCI bus), Galil's DMC-1842 motion controller inside the personal computer and WSDK software, ICM-2900 Interconnect Module (e), two servo motors (f and g) (a Pitmann 19.1 V DC servo motor at elbow and Motor-50-100 at the base), 24VDC 6 A power supply (h), two MSA12A8 servo amplifiers (i) for each motors.

In Fig. 9(a), for the laboratory implementation, Galil's DMC-1842 motion controller generates command signals, and requests status updates from the built in encoders in the electric motors. The ICM-2900 Interconnect Module provides easy connections between the controller, amplifiers and encoders. The two servo motors located at the elbow and the base of the two-link arm implement the control action by serving as

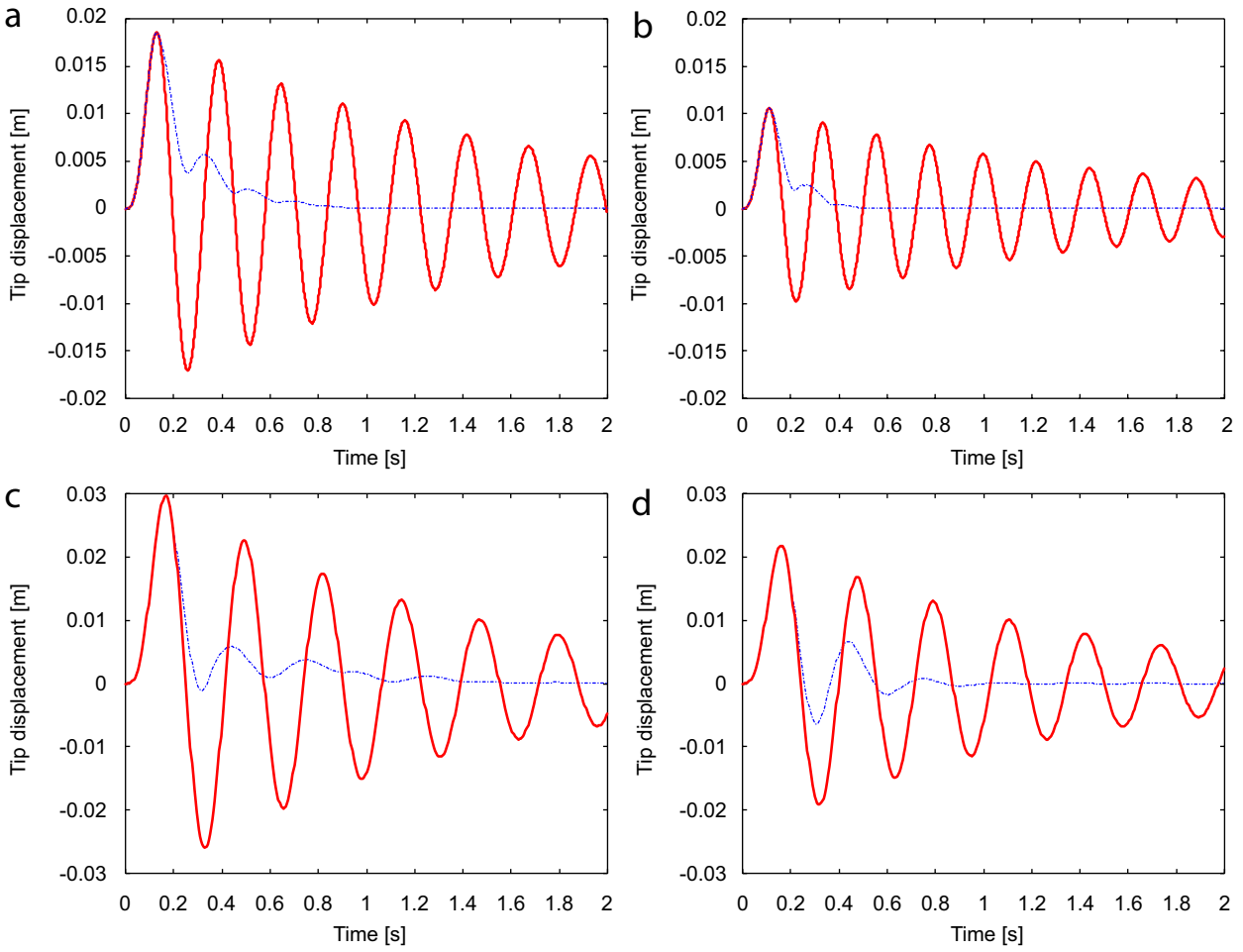

Fig. 8. Tip displacement histories of uncontrolled (——) and dual controlled (–·–·–·–) cases for different arm lengths of (a and c) $L_1 = 0.2\,\text{m}$, $L_2 = 0.5\,\text{m}$, (b and d) $L_1 = 0.5\,\text{m}$, $L_2 = 0.2\,\text{m}$ at elbow angle $\alpha = 0^\circ$ ((a) and (b) are for rigid linkages-flexible joints, (c) and (d) are for flexible linkages-flexible joints model.).

torsional springs. These servo motors have built-in encoders that serve as sensors to obtain the history of the angular displacement and velocity at each joint and communicate with the controller. Base motor's encoder has a resolution of 4000 steps per revolution (± 0.0008 rad) and the elbow motor's encoder has a resolution of 2000 steps per revolution (± 0.0016 rad). Two MSA12A8 servo amplifiers suitable for small motors boost the controller's signals to a level which is sufficient for driving the motors.

The objective of the control scheme is to implement the VSC technique to an existing position controller, Galil motion controller, which operates on the basis of proportional-integral-derivative (PID) filter. The details of programming and operation of the controller can be found in Ref. [24]. As mentioned in Section 2, along with the energy dissipation outcome of the control action, the effect of an actuation is a shift of the equilibrium position that produces an opposing force to the velocity of oscillations. Thus, the VSC can be implemented in two different ways. One is to apply a constant opposing torque, and the other is to shift the equilibrium position of the torsional springs. Shifting the equilibrium position is chosen here considering the fact that an application of a torque has always a chance to de-stabilize the control process. In addition, this way of implementation is more convenient from the viewpoint of programming. A stiffness ratio, $\Delta K/K = 0.5$, is equivalent to shifting the equilibrium position by half of the peak displacement. Accordingly, during the experiments, the implementation of the control has been achieved by shifting the equilibrium position of the electrical motors by half, as soon as a velocity sign change has been observed.

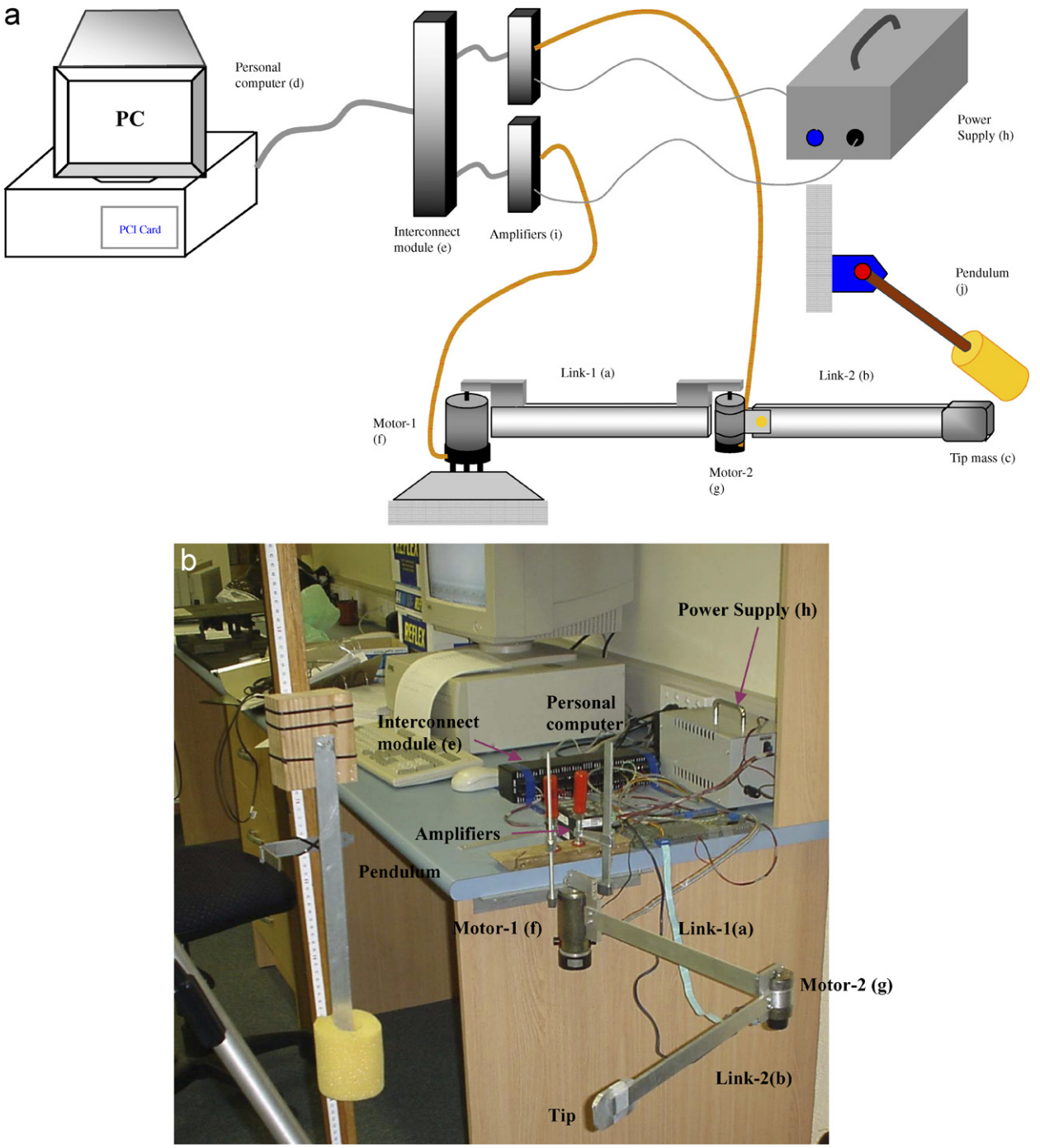

Fig. 9. (a) Schematic of experimental setup and (b) photograph of laboratory setup.

The experiments start with striking the tip of the arm with a simple pendulum by releasing it from a predetermined height as shown in Fig. 9(b). This simple pendulum setup provides a consistently repeatable transient disturbance. The tip impact is assumed to act for a relatively short time. Such forces are impulsive and result in a sudden change to the system's initial velocity [20]. Therefore, the effect of this disturbance has been approximated by an equivalent initial velocity at the tip of the arm during simulations.

The servo motors can be programmed to behave like torsional springs via a custom coded program [24]. Angular positions, velocities or accelerations of each electrical motor can be monitored through the built-in encoders. As soon as a velocity sign change is detected, a peak angular displacement is assumed to exist, and an actuation is imposed by shifting the equilibrium position by half immediately following the instant of the peak displacement. Time increment of 40 ms has been employed to capture each data and provide an intentional delay to actuations after each control action (similar to a moving-average filtering). The measured data from the built-in encoders are then used for graphical presentation and analyses of angular displacement histories of each electrical motor in MATLAB environment [21].

3.2. Experimental results

Similar to Section 2, the results have been obtained for different elbow angles, α, of 0°, 30°, 60°, 90° and 120° for uncontrolled, only-base controlled, only-elbow controlled and dual controlled cases. Numerical simulations have been performed to compare with the experimental observations for dual controlled and uncontrolled cases. Numerically suggested best stiffness ratio, $\Delta K/K = 0.5$, has been validated experimentally by varying stiffness ratios between 0.1 and 0.9 for different elbow angles, [23]. Only the representative results will be demonstrated here for brevity.

The parameters used in experiments are listed in Table 4. The effective stiffness values of each motor in Table 4 and equivalent viscous damping coefficients are determined by attaching a rigid single-link on each electrical motor and obtaining the displacement histories in response to a transient disturbance. The effective stiffness values for the electrical motors are then calculated from the natural frequencies. The viscous damping coefficients are obtained by using the logarithmic decrement. With these experimental parameters, the fundamental frequency of the prototype arm ranges between 2.47 rad/s and 3.42 rad/s for the elbow angles between 0° and 120°, Table 5.

Numerical predictions (——) and the experimental observations (–·–·–·–) for uncontrolled and dual controlled cases, are presented in a similar format in Figs. 10(a)–(u) and 11(a)–(u) for the elbow angles, α, of 0°, 30°, 60°, 90°, and 120°. The comparisons clearly indicate that the numerical predictions are able to capture the significant trends in the control action. In general, uncontrolled experimental cases have oscillations at slightly lower frequencies and decay quicker than the numerical predictions. This difference between

Table 4
Experimental two link-arm parameters

Arm parameters	
Length, L_1	0.418 m
Length, L_2	0.351 m
Width of beam, b_1	0.032 m
Width of beam, b_2	0.025 m
Thickness of beam, h_1	0.003 m
Thickness of beam, h_2	0.006 m
Bending stiffness of beam, EI_1	5.18 N m^2
Bending stiffness of beam, EI_2	32.4 N m^2
Mass/length of beam, m_1	0.49 kg/m
Mass/length of beam, m_2	0.46 kg/m
Number of finite elements for each link	10
Other parameters	
Tip mass, M_{tip}	0.055 kg
Actuator mass, M_{motor}	0.310 kg
Passive elbow stiffness, K_{elbow}–ΔK_{elbow}	0.08 N m/rad
Active elbow stiffness, ΔK_{elbow}	0.08 N m/rad
Passive base stiffness, K_{base}–ΔK_{base}	0.77 N m/rad
Active base stiffness, ΔK_{base}	0.77 N m/rad
Equivalent viscous damping ratio—structural	0.005
Elbow viscous damping coefficient	0.001 N m/rad/s
Base viscous damping coefficient	0.002 N m/rad/s

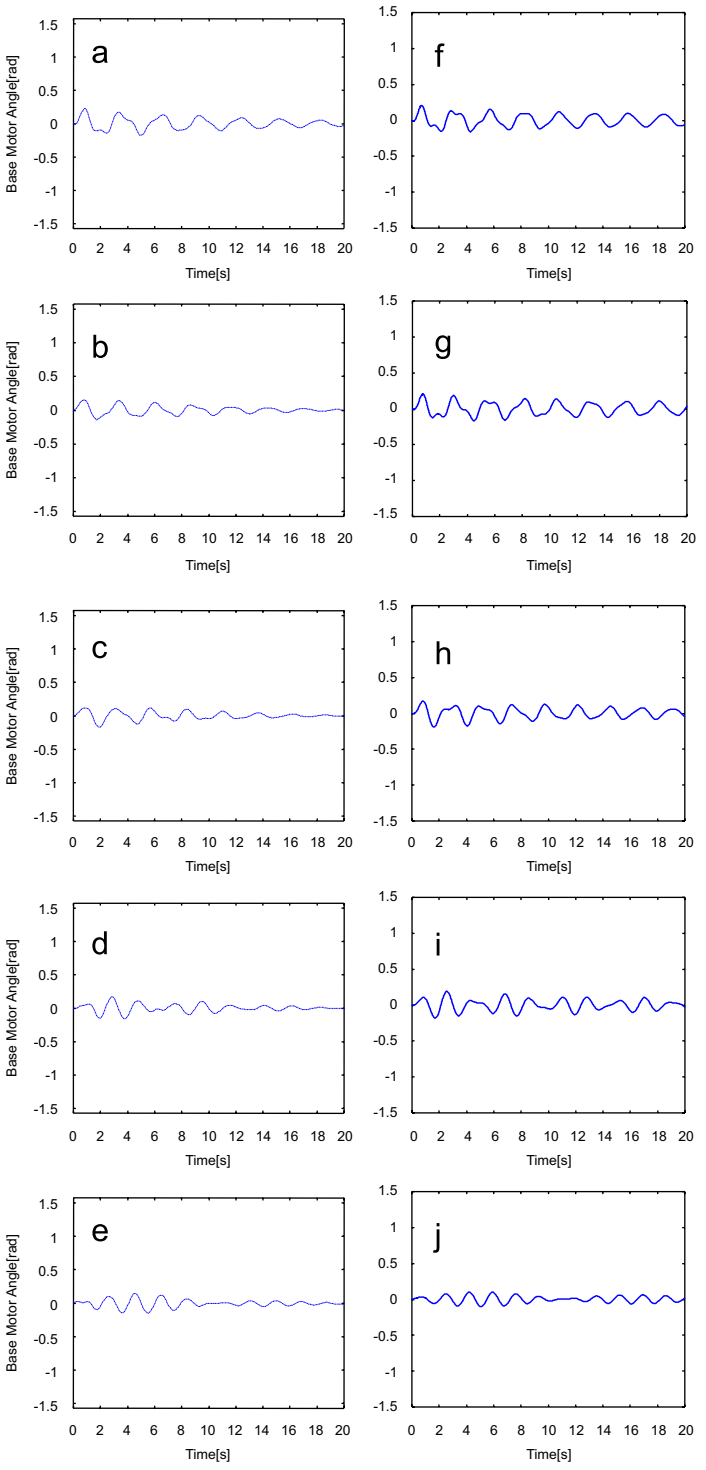

Fig. 10. Comparison of uncontrolled experimental (–·–·–·–) and uncontrolled numerical (——) base and elbow histories ((a) to (e) for experimental base; (f) to (j) for numerical base; (k) to (o) for experimental elbow; (p) to (u) for numerical elbow). Each row corresponds to an elbow angle of 0°, 30°, 60°, 90° and 120°, in descending order.

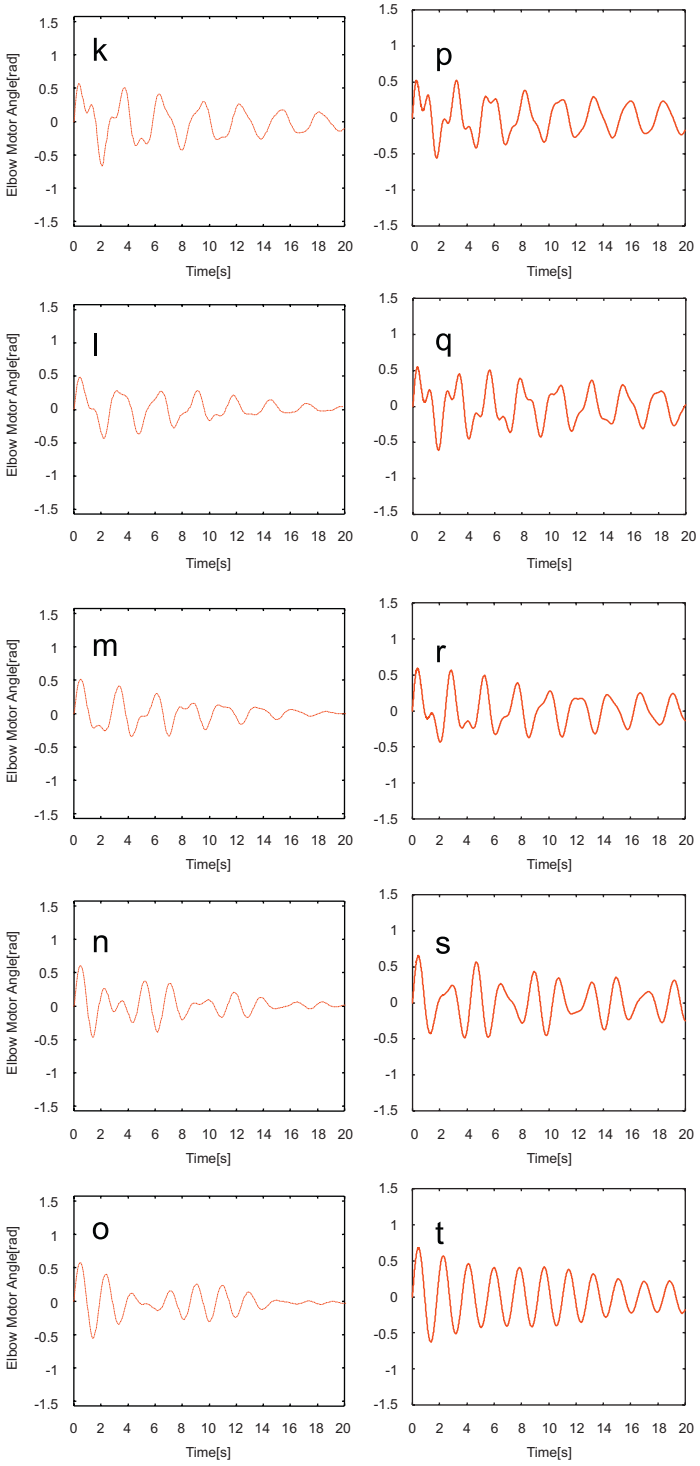

Fig. 10. (*Continued*)

experimental and numerical results for uncontrolled cases may be reasoned to be due the presence of frictional resistance which is not properly included in the numerical model where the two links are attached (the damping coefficient for the numerical model have been obtained by measuring the response of a single-link

attached to a motor). Nevertheless, both the dual controlled and uncontrolled cases collectively present similar trends. In Fig. 11, improvements are clear for the dual controlled experiments similar to the numerical predictions. Vibration energy of the robotic arm during experiments is dissipated within about one and a half cycle, which is around 4 s. at almost all configurations of the robotic arm. The experimental results for the dual controller cases prove that the controller is effective and versatile in a wide range of elbow angles.

Similar to the numerical simulations, histories of the relative elbow angle and base angle for uncontrolled, only-elbow and only-base controlled cases have been performed for different elbow angles, α, of 0°, 30°, 60°,

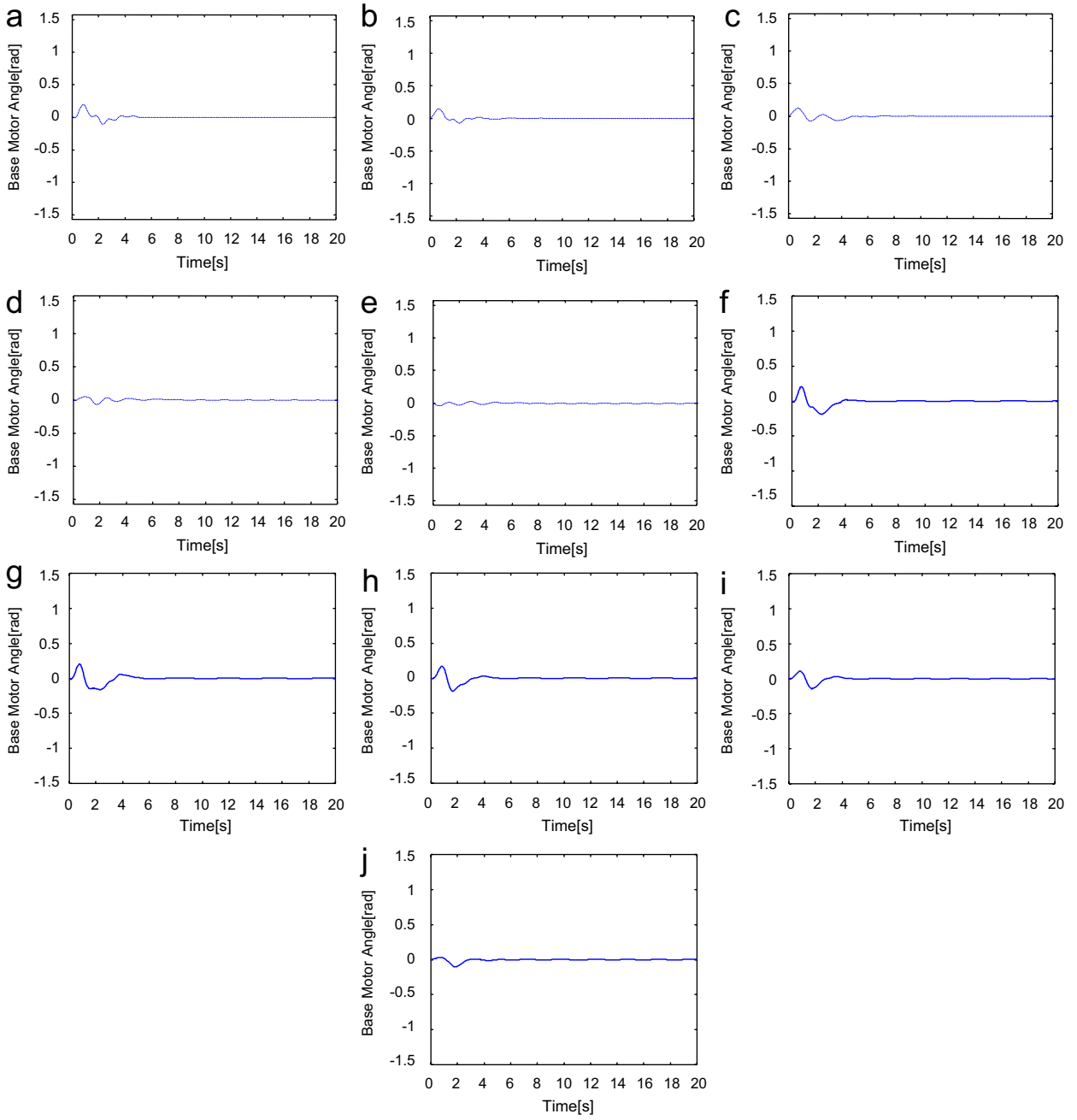

Fig. 11. Same as in Fig. 10, but for dual control.

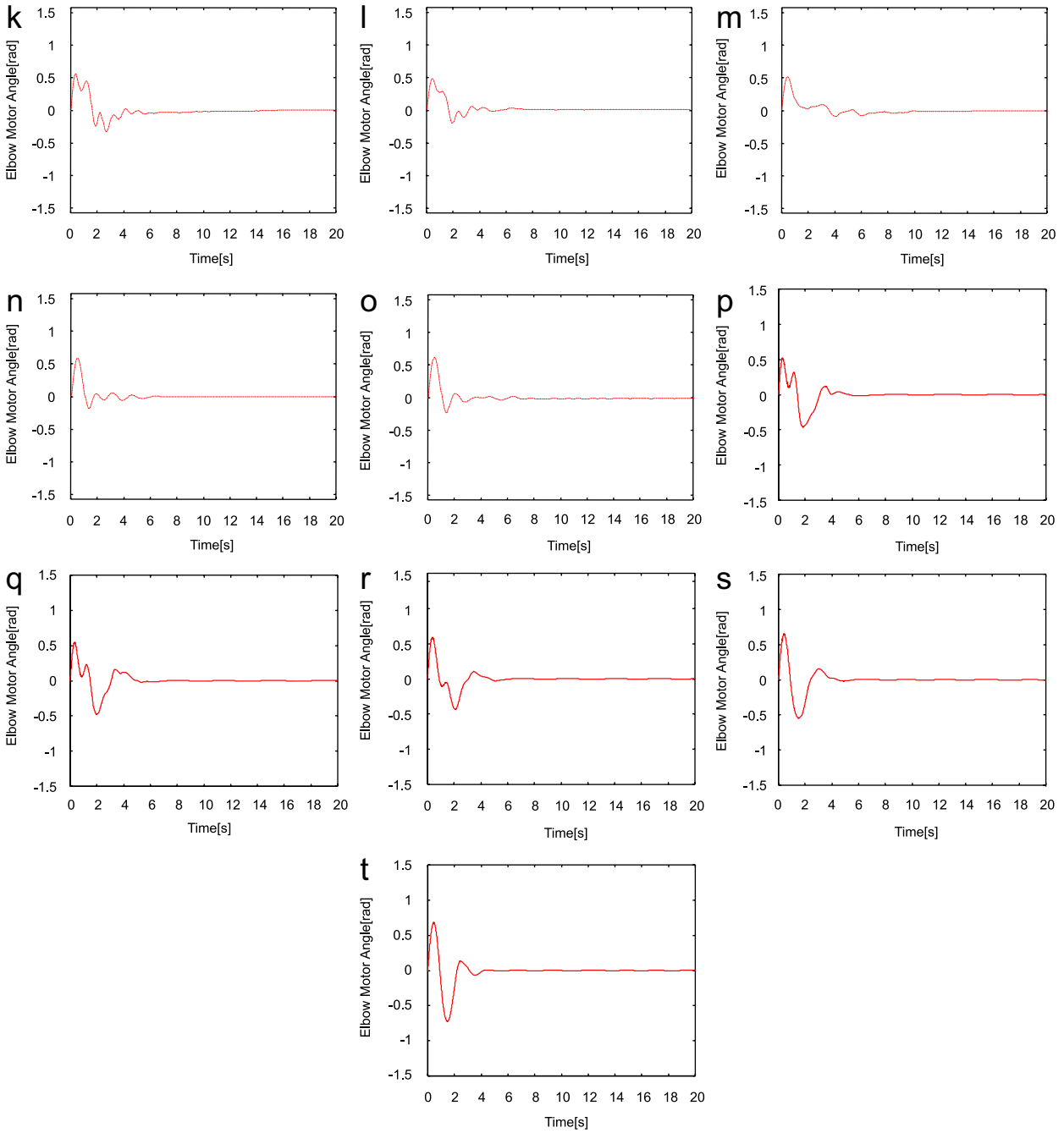

Fig. 11. (*Continued*)

90°, and 120°, respectively. Similar conclusions to those obtained during numerical simulations have been observed with the experimental observations [23].

Finally, as an interesting case study, experiments have been performed with an extremely flexible link-2. Results are given in Figs. 12(a)–(d) for uncontrolled and controlled cases with the same experimental parameters as above except the Link-2. In this case the Link-2 length has been replaced with a relatively long and flexible slender beam (0.8 m, with a cross-section of 1 mm × 52 mm and material of aluminum). Considering the control is only achieved at joints to dissipate energy, the flexural vibrations of the links may

Table 5
Natural frequencies of the system for different elbow angles obtained from simulations

Elbow angle (deg)	ω_1 (rad/s)	ω_2 (rad/s)
0	2.47	6.29
30	2.56	5.86
60	2.71	5.03
90	3.03	4.34
120	3.42	3.99

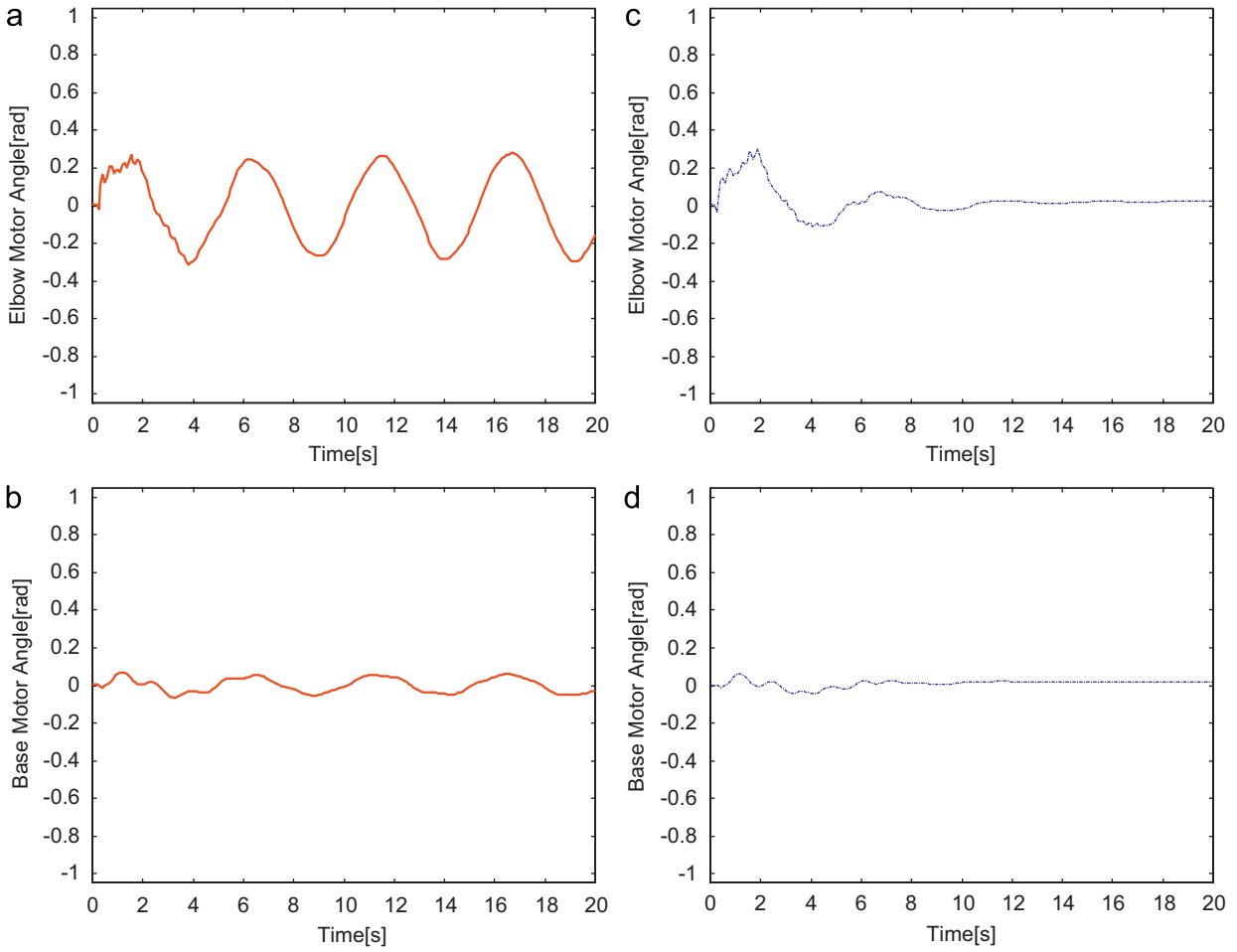

Fig. 12. Experimental elbow and base displacement histories for uncontrolled (——) (a and b) and dual controlled (–·–·–·–) (c and d) cases for robotic arm with extremely flexible link-2 for an elbow angle of 0°.

be expected to be prolonged due to the higher frequencies excited in the system. However, even with the very flexible linkages, experiments show a comparable success in achieving the control relatively quickly.

4. Conclusion

In this paper, variable stiffness controller (VSC) technique has been proposed and tested on a two-link flexible robot arm model. Comparison between the dual controller and single-controller has been presented

with numerical simulation results. The controller's performance has been compared through numerical simulations in changing circumstances such as orientation of arm or link parameters. Throughout the extensive simulations for a two-link flexible robot arm model, the controller has proven itself as a promising, versatile control technique for robotic applications. Its suitability to changing circumstances and parameters without additional hardware, complexity or cost makes the proposed controller distinct from all other active control techniques. One of the most important characteristics of the VSC technique has been verified that the control action is unconditionally stable since the technique is based on dissipating energy from the system.

Experiments have been conducted on a laboratory prototype robotic arm to validate the versatility and effectiveness of the proposed technique. Numerical predictions have been verified through extensive comparisons. Numerical and experimental results prove that quick attenuation of the system oscillations can be obtained robustly with the proposed controller without any additional hardware.

References

[1] W.J. Book, Controlled motion in an elastic world, *ASME Journal of Dynamic Systems, Measurement and Control* 113 (1993) 252–261.
[2] G.B. Andeen editor in chief, *Robot Design Handbook*, McGraw-Hill Book Company, New York, 1988.
[3] D. Wang, M. Vidyasagar, Passive control of a stiff flexible link, *The International Journal of Robotics Research* 11 (12) (1992) 572–578.
[4] S. Hong, Y. Park, Vibration reduction for flexible manipulators using torque wheel mechanism, *Proceedings of the Third International Conference on Motion and Vibration Control, Chiba, Japan*, 1996, pp. 364–369.
[5] W. Bernzen, Active vibration control of flexible robots using virtual spring-damper systems, *Journal of Intelligent and Robotic Systems* 24 (1999) 69–88.
[6] B. Siciliano, Closed-loop inverse kinematics algorithm for constrained flexible manipulators under gravity, *Journal of Robotic Systems* 16 (6) (1999) 353–362.
[7] J. Yuan, Robust vibration control based on identified models, *Journal of Sound and Vibration* 269 (2004) 3–17.
[8] S.Y. Lim, D.M. Dawson, J. Hu, M.S. Querioz, An adaptive link position tracking controller for rigid-link flexible-joint robots without velocity measurements, *IEEE Transactions on Systems, Man and Cybernetics—Part B: Cybernetics* 27 (3) (1997).
[9] G. Bartolini, W. Caputo, M. Cecchi, A. Ferrera, L. Fridman, Vibration damping in elastic robotic structures via sliding modes, *Journal of Robotic Systems* 14 (9) (1997) 675–696.
[10] N.D. Maxwell, S.F. Asokanthan, Modal characteristics of a flexible beam with multiple distributed actuators, *Journal of Sound and Vibration* 269 (2004) 19–31.
[11] Z. Mohamed, M.O. Tokhi, Command shaping techniques for vibration control of a flexible robot manipulator, *Mechatronics* 14 (2004) 69–90.
[12] L.Y. Lu, Semi-active modal control for seismic structures with variable friction dampers, *Engineering Structures* 26 (2004) 437–454.
[13] J.H. Kim, C.W. Lee, Semi-active damping control of suspension systems for specified operational response mode, *Journal of Sound and Vibration* 260 (2003) 307–328.
[14] Q. Zhou, S.R.K. Nielsen, W.L. Qu, Semi-active control of three-dimensional vibrations of an inclined sag cable with magnetorheological dampers, *Journal of Sound and Vibration* 296 (2006) 1–22.
[15] Y. Liu, T.P. Waters, M.J. Brennan, A comparison of semi-active damping control strategies for vibration isolation of harmonic disturbances, *Journal of Sound and Vibration* 280 (2005) 21–39.
[16] J. Onoda, T. Endo, H. Tamaoki, N. Watanabe, Vibration suppression by variable-stiffness members, *American Institute of Aeronautics and Astronautics Journal* 29 (6) (1991) 977–983.
[17] A. Warkentin, S.E. Semercigil, Variable stiffness control of a single-link flexible robotic arm, *Journal of Sound and Vibration* 187 (1) (1995) 1–21.
[18] J. Pun, S.E. Semercigil, Joint stiffness control of a two-link flexible arm, *Nonlinear Dynamics* 21 (2) (2000) 173–192.
[19] K.J. Bathe, *Finite Element Procedures in Engineering Analysis*, Prentice-Hall, Englewood Cliffs, NJ, 1982.
[20] W.T. Thomson, *Theory of Vibrations with Applications*, fourth ed, Prentice-Hall, Englewood Cliffs, NJ, 1993.
[21] Matlab, *MATLAB, The Language of Technical Computing, Using MATLAB Version 5*, The MathWorks, Inc, MA, 1997.
[22] R.R. Craig, *Structural Dynamics, An Introduction to Computer Methods*, Wiley, USA, 1981.
[23] A. Özer, Vibration Control of Flexible Robot Manipulators, Ph.D. Dissertation, Victoria University of Technology, Melbourne, Australia, 2005.
[24] DMC-18 × 2 Manual Rev. 1.0d, Galil Motion Control, Inc., California.